Characteristics and performance of wind profiles as observed by the radar wind profiler network of China

Boming Liu,[1,+] Jianping Guo,[2,+] Wei Gong,[1] Lijuan Shi[3], Yong Zhang[3] and Yingying Ma[1]

[1] State Key Laboratory of Information Engineering in Surveying, Mapping and Remote Sensing (LIESMARS), Wuhan University, Wuhan, China
[2] The State Key Laboratory of Severe Weather, Chinese Academy of Meteorological Sciences, Beijing 100081, China
[3] Meteorological observation Centre, Chinese Meteorological Administration, Beijing 100081, China
[+] The authors contributed equally to this work

Correspondence to: Jianping Guo (jpguocams@gmail.com)

Abstract. Wind profiles are fundamental to the researches and applications in boundary layer meteorology, air quality, and numerical weather prediction. Large-scale wind profiles data have been previously documented from network observations in several countries, such as Japan, USA, various European countries and Australia, but the nationwide wind profiles observations are poorly understood in China. In this study, the salient characteristics and performance of wind profiles as observed by the radar wind profiler network of China is investigated. This network consists of more than 100 stations instrumented with 1290-MHz Doppler radar designed primarily for measuring vertical-resolved winds at various altitudes but mainly in the boundary layer. It has good spatial coverage, with much denser sites in coastal areas. The wind profiles observed by this network can provide the horizontal wind direction, horizontal wind speed, and vertical wind speed for every 120 m interval within the height of 0 to 3 km. The availability of the radar wind profiler network has been investigated in terms of effective detection height, data acquisition rate, data confidence, and data accuracy. Further comparison analysis with reanalysis data indicated that the observation data at 89 stations are recommended, and 17 stations are not recommended. The wind profiles can serve as important input dataset assimilated into numerical weather prediction systems at both regional and global scales.

1 Introduction

It is increasingly recognized that the atmospheric wind profiles and its vertical wind shear are crucial to better understanding the more frequent extreme rainfall events (Huuskonen et al., 2014; Nash and Oakley, 2001; Weber et al., 1990), intensification of clear-air turbulence associated with aircraft safety (Williams & Joshi, 2013), complicated aerosol-cloud-precipitation interaction (Fan et al. 2009; Guo et al. 2016a; 2019; Lee et al., 2016), and persistent particulate pollution episodes (Yang et al., 2019; Zhang et al., 2020). For the wind speed in the planetary boundary layer (PBL), the most striking feature is that the turning of winds with height dominates the whole PBL and beyond, which can be explained in terms of force vectors (drag, pressure gradient force, Coriolis force) at the surface and the top of the PBL (pressure gradient force and Coriolis force) (Lemone et al., 2018). Under influences of large-scale dynamic forcing and land surface process, wind speed and direction will dramatically vary (Michelson & Bao, 2008), which poses a large challenge for models to simulate or forecast the variation of wind very well, especially in the PBL (Constantinescu et al., 2009; Guo et al., 2016b).

Radar wind profiler (RWP), which is generally Doppler radar that operates at either the VHF (30-300 MHz) or UHF (300-1000 MHz) frequency bands, has been widely applied to atmospheric wind field research (Dolman et al., 2018; Molod et al., 2015; Ishihara et al., 2006; Schlatter et al., 1994). To date, a large spectrum of field campaigns involved with the RWP observed wind profiles, especially over the regions with intensive anthropogenic and industrialized activities, have been conducted and their archived dataset has been increasingly receiving attention (Liu et al., 2019; Kottayil et al., 2016; Singh et al., 2016; LeMone et al., 2013; Bianco et al. 2008; Le et al., 1998), most of which are based on ground-based remote sensed measurements. The earliest space-borne wind products generally refer to the atmospheric motion vectors that are derived by tracking clouds or areas of water vapor through consecutive infrared remote sensing images (Schmetz et al., 1993; Velden et al., 2005). Later on, the vector winds over the ocean surface have been measured by the spaceborne microwave instruments such as SeaWinds onboard QuikSCAT (Bentamy et al., 1999; Draper and Long 2002). Since 2018,

new satellite-based wind observational era set in with the launch of European space agency (ESA)'s Aeolus wind satellite on which the direct-detection Doppler wind lidar ALADIN is accommodated, which provides line-of-sight winds along the satellite track (Reitebuch et al., 2009; Reitebuch 2012). As of 12 May 2020, the Aeolus data has gone public after the bias correction of the winds has been adequately made, which are now being distributed publicly to forecasting services and scientific users in less than three hours of measurements being made from space (https://www.esa.int/Applications/Observing_the_Earth/Aeolus/Aeolus_goes_public). Moreover, aircraft-based observation of atmospheric wind profiles has been carried out worldwide (Lux et al., 2018; Marksteiner et al., 2018; Witschas et al., 2017; Chouza et al., 2016; Weissmann et al., 2005). Especially in the North Atlantic Waveguide and Downstream Experiment (NAWDEX) campaign, the ALADIN team conducted several airborne wind measurement experiments for the validation of the Aeolus satellite winds product (Lux et al., 2020; Zhai et al., 2020).

To gain a full picture of regional scale wind fields, a number of RWP networks have been set up across the world. As early as 1990s, the demonstration wind profile network is deployed and maintained by the National Oceanic Atmospheric Administration (NOAA), which is also termed NOAA profiler network (NPN) and operated at a frequency of 404 MHz (Schlatter et al., 1994; Vande Kamp, 1993; Weber at al., 1990). The second type of profiler is the 915-MHz boundary-layer profiler that is much smaller, transportable, commercially available but lacked height coverage compared with 404 MHz wind profiler, and thus is mainly used for NOAA research and outside agencies. Nevertheless, probably due to the fact that the RWP reached the end of their useful lives, the NPN largely ceased to operate in 2014 and the last stations closed in 2017. As an alternative data source, the high-density airborne wind and temperature profiles from civil aviation industry gradually took over the role of RWP since then (https://madis.ncep.noaa.gov/madis_npn.shtml). To make the most out of the best sampling attributes of the abovementioned two types of wind profiler, a third type of profiler operated at 449 MHz. Later on (in 1996),

the European Cooperation in Science and Technology framework (COST) initiated the project of Wind Initiative Network Demonstration in Europe (CWINDE). Under the framework of CWINDE, the European RWP network named E-PROFILE, as part of the EUMETNET Composite Observing System (EUCOS), is constructed, providing the monitoring of vertical profiles of wind across Europe (Dibbern et al., 2001; Oakley et al., 2000; Nash and Oakley, 2000). Moreover, the Japan Meteorological Agency developed the operational wind profiler network in Japan in 2011, which is a nationwide network of 33 wind profiler currently in operation. The wind data have significant positive impact on improving numerical weather prediction (Ishihara et al., 2006). The Australian Bureau of Meteorology completed the installation of the Australian wind profiler network of 19 wind profiler in 2017 that runs at 55 MHz frequency band, which produces wind data of sufficient accuracy for presentation to forecasters and ingestion into global numerical weather prediction models (Dolman et al., 2018). The aforementioned networks have provided vertical profiles of wind for model assimilation through the Global Telecommunication System at regional or national scale (e.g., Benjamin et al., 2004; Chipilski et al., 2019), which was found to significantly improve the forecast of rainfall onset and atmospheric pollution episode (Liu et al., 2019; Liu et al., 2018; Singh et al., 2016; LeMone et al., 2013; Du et al., 2012; Bianco et al. 2008; Angevine et al., 1994).

Given the considerable advantages over conventional ground-based in situ or remote sensing observations, wind profiler measurements have been well applied in a variety of applications in China, including air quality and weather forecast (Sun, 1994; Hu et al., 2010; Dong et al., 2011; Miao et al. 2018; Zhang et al., 2020). Nevertheless, the RWP is generally deployed at either specific regions or short time period. Recent model simulation work by assimilating wind measurements from a regional wind profiler network in North China indicated the network observation significantly improved the convective forecasting (Wang et al., 2020). Meanwhile, the extreme precipitation is continuously intensified under global warming and deteriorated atmospheric pollution, especially in Eastern Asian countries such as China and India (Zhang et al., 2006; Pfahl et al., 2017; Guo et al., 2019; Li et al.,

2020), which desperately needs the vertical wind observations. However, the characteristics and performance of nationwide profiler network in China has never been revealed, and the assessment of systematic observation performance and data accuracy are still lacking, to the best of our knowledge. This motivates us to evaluate the performance and accuracy of RWP network of China, ultimately in an attempt to present a wind profile data as a new data source for numerical weather prediction or climate related studies. The remainder of this paper is organized as follow. The RWP network of China is briefly introduced in Section 2. The performance and accuracy are evaluated in Section 3. Section 4 will discuss the detailed application of wind profile data. A summary of results is presented in Section 5.

2 Description of the RWP network

This network began to be constructed dating back to 2008, when there are 5 sites having wind profiling measurements transmitted to the headquarter of China Meteorological Administration (CMA). The number of RWP sites continuously increased to 92 at the end of 2017, all of which are operating at 405 MHz frequency band. The RWP network of China is comprised of 106 stations until March 2019, which is designed primarily for measuring winds at various altitudes. Afterwards, the working frequency band is changed to L band (1290 MHz), and the number increased to 128 at February 2020 (personal communication with Dr. Ruiyi Li from CMA). The Meteorological Observation Center (MOC) of CMA is responsible for the operation and maintenance of the nationwide wind profiler network. Table 1 shows the instrument information of RWP used in this study, which consist of three types of RWP: high troposphere, low troposphere and boundary layer RWPs. It can be seen that the majority of the radars are boundary layer RWP operating at L band (101 sites), and a few of sites are instrumented with tropospheric RWP operating at P band (5 sites). Fig. 1 shows the spatial distribution of wind profiler network in China, which exhibits large spatial domain extending from the northernmost site located at Wulumuqi at 43.0°N, to the southernmost one at Nanhai at 17.0°N, and

from the westernmost site also located at Wulumuqi at 87.0°E to the easternmost one in Shenyang at 123.0°E. The detail information of the RWP network of China is shown in Table S1.

The MOC/CMA is responsible for the maintenance and collection of wind measurements from the wind profiler network, as shown in Fig. 2. Specifically, the data transfer from radar sites to MOC/CMA is mainly done using Internet connections. The data center of CMA is established to efficiently process the data collected by Internet. There are two main types of data collected from the wind profilerr network: raw data and product data. The former data includes the power spectrum data files (indicated by FFT) and radial data files (indicated by RAD). The power spectrum data file is composed of file identification, basic parameters of the station, performance parameters, observation parameters and observation data. The power spectrum data file is dynamically generated in real time according to demand. The radial data files are twofold: one is reference information, such as the basic parameters of the station, radar performance parameters, and observation parameters; the other is the observation data of each beam at each sampling height, including sample height, velocity spectrum width, signal-to-noise ratio, and radial velocity. As for the product data, three main wind profile products are produced by the data center of CMA: (1) Real-time sampling data file (at 6-min intervals), mainly including the sampling height, horizontal wind direction, horizontal wind speed, vertical wind speed, horizontal credibility, vertical credibility, and Refractive Index Structure Parameter (C_n^2). An individual file will be produced for every 6-min detection and is marked as ROBS. (2) Half-hour data file (at 30-min intervals), which is broadly consistent with ROBS file in terms of both data content and format, except for the file produced for every half hour (48 files per day), and the file is marked as HOBS. (3) One-hour observation sampling data file (at 60-min intervals) with 24 files per day, which is marked as OOBS.

These wind profile products are generated for each observation site. The vertical resolution of wind profile data at most sites is 120 m. However, a few sites use a low-level detection mode with high sampling rate, these provide a vertical resolution of 60 m. Examples of wind profile product are shown

in Fig. 3. Seven different heights (150, 500, 1000, 1500, 2000, 2500, and 3000 m) are selected to show the atmospheric vertical wind field (Fig. 3e). It can provide the vertical profiles of horizontal wind direction, horizontal wind speed, and vertical wind speed. Those products are available for official duty use and for research and education. The observation data from November 2018 to March 2019 are used to evaluate the performance of the RWP network of China. Due to the fact that the measurements from the China RWP network have to be further assessed, the data sharing via global telecommunications system is expected to occur in the next several years, which highly depends on the process of data quality assessment.

3 Performance of the RWP network

The RWP network of China includes a variety of types of RWPs, including high troposphere, low troposphere and boundary layer RWPs. Due to the algorithms and setting parameters of different instruments are inconsistent, the system performance index and data accuracy are inhomogeneous. Therefore, it is necessary to evaluate the system performance index and data accuracy of the radars in the RWP network. This is a major step forward in the harmonization of the product generation and data quality of the RWP network of China. Three system performance indicators on data application are investigated, including effective detection height, data acquisition rate, and data confidence. In order to estimate the data accuracy, the wind profiles from RWP are compared with hourly wind measurements at 0.25 x 0.25-degree latitude/longitude grid from the fifth generation European Centre for Medium-range Weather Forecasts (ECMWF) atmospheric reanalysis of the global climate (ERA5, Hoffmann et al., 2019).

3.1 System performance index

The operation mode of the RWP network includes high, medium, and low detection modes, which can detect wind field information at different altitudes. High mode is generally used to detect the wind

fields at a height of 5–10 km above ground level (AGL). The medium and low modes is used to detect wind fields at a height of 0–5 km above the ground. We here define "effective detection height" as the effective detection height up to where wind measurements are available. Fig. 4a, b show the mean effective height detected by each RWP during the period from November 2018 to March 2019. There are 90 stations with an average height greater than 3 km; 10 of them can even reach more than 7 km. As for the acquisition rate, it refers to the ratio of the actual acquisition time to the total theoretical acquisition time, which is used to evaluate the normal operation of the wind profile radar. Fig. 4c, d represent the data acquisition rate of wind measurement at RWP network during the period from November 2018 to March 2019. The data collection rate of most sites is greater than 90%, while the data collection rate of 4 sites is less than 50%. Fig. 4e, 4f represent the average confidence of wind measurement at RWP network. Confidence is a credible parameter set by the system for the wind speed information at each sampling point, which is used to evaluate the credibility of the wind field information retrieved at each altitude position. The results indicate that there are 100 sites with more than 90% confidence, but 6 sites have less than 90% confidence.

In order to make the criteria of RWP network data consistent, we have to set corresponding screening criteria for each system index, which to some degrees reflects the needs of future applications. For instance, the RWP network data are expect to be used to derive boundary layer parameters, such as boundary layer height (Liu et al., 2019) and wind shear that are closely related to atmospheric pollution (Zhang et al., 2020). Therefore, it would be better for the effective detection height of RWP reaching 3 km, with the acquisition rate being above 60%. In addition, according to the user manual of RWP, only those wind profile data with a 100% confidence level are recommended. According to these criteria, the wind profile data at each site are screened, and the screening results are shown in Fig. 5. Fig. 5a shows the results of screening for effective detection height. The results show that the effective height detected by RWP of 102 stations meets this standard, and 4 stations are not up to the standard. The substandard sites are 54752, 58365, 58474, 58730. Fig. 5b shows the screening results of the data

acquisition rate. The results show that the data acquisition rate of 100 sites is satisfactory, and 6 sites are not up to standard. These substandard sites are 16078, 58158, 58460, 58927, 58933 and 59431. Fig. 5c shows the results of the confidence level screening. The results show that 100 sites are up to standard and 6 sites are substandard. The substandard sites are 54727, 54736, 54857, 57494, 58365 and 58460. Overall, 92 sites of the RWP network have a good system performance.

3.2 Data accuracy

The echo signal from RWP can be processed to provide the wind profile at RWP sites. However, it should be noted that the accuracy of wind profile data is also closely related to the processing algorithm. Therefore, the work to check the accuracy of the data is necessary before using these observations. The comparison statistics against the wind profile data from ECMWF numerical model is an important monitoring tool (Huuskonen et al., 2014). Fig. 6 shows the comparison results between wind profile from RWP and that from ECMWF at six stations. The vertical validation range is from 0 to 3 km. The mean speed difference (MSD) and root-mean-square difference (RMSD) of horizontal wind speed between RWP and ECMWF (RWP–ECMWF) are calculated at each height. The red and blue dot lines represent the MSD and RMSD at different heights, respectively. The vertical distribution of MSD at different sites is different, but almost of MSDs are less than 5 m/s. It is clear that a discrepancy does not automatically imply that the wind profile is in error, but in general a gross deviation with the model results can be considered as an indication of a radar error. Ishihara et al. (2006) evaluated the wind accuracy of Japanese RWP network by comparisons with the numerical weather prediction model profiles, and the RMSD are around 3 m/s. Huuskonen et al. (2014) compared the wind profiles observed by EUMETNET with the ECMWF model profiles, and set 5 m/s RMSD as a target for acceptable wind observations.

Here, the horizontal wind speed measurements at all levels ranging from 0 to 3 km are used to calculate the MSD and RMSD at each site. Moreover, the magnitude of mean speed difference (MMSD) and

RMSD are set to be 4 m/s and 6 m/s, respectively, which serve as a target for acceptable criterion. Fig. 7 shows MMSD and mean RMSD from 0 to 3 km for all RWP, calculated by comparing with ECMWF wind data. It is seen that most of RWP meet consistently the acceptance criterion of 4 m/s MMSD and 6 m/s RMSD, while few radars also show larger differences. Moreover, the MMSD and RMSD of RWP network has a certain spatial difference. According to the average difference in zonal direction (histogram in Fig.7), the RWPs at 28-32°N area have relatively large difference, where the zonal MMSD is larger than 2 m/s and zonal mean RMSD is larger than 5 m/s. The sites with MMSD greater than 4 m/s include 54857, 57494 and 59046; and the sites with RMSD greater than 6 m/s include 52889, 57494, 58448 and 59046. The wind data at these sites have large difference and are not recommended. The large difference may be caused by either hardware or configuration problems, such as the aging of components. Therefore, it is important to conduct regular maintenance and replacement of aged components. In addition, there are eleven wind profile radar sites which are equipped with radiosonde (51463, 54342, 54511, 54727, 54857, 57494, 57516, 58238, 59758, 59948, and 59981).

Overall, the availability of RWP network of China can be evaluated by combining the system performance index and data accuracy. Fig. 8 shows the spatial distribution and number of recommended and non-recommended sites. The availability of RWP network of China is 84%, which 89 stations are recommended, and 17 stations are not recommended. These non-recommended sites include: 16078, 52889, 54752, 54727, 54736, 54857, 57494, 58158, 58365, 58448, 58460, 58474, 58730, 58927, 58933, 59046, and 59431. For the sites with low height coverage or low data acquisition rate, the data availability can be improved by changing the radar observation modes and increasing radar runtime. But for the sites with low confidence level or low data accuracy, which is caused by the inversion algorithm or the instrument system, it needs to choose the appropriate optimization method for specific problems. Some methods on data quality control are given in previous studies (Holleman, 2005).

4 Applications of the RWP network

4.1 Daily maximum winds

The wind profile data can be used to monitor the diurnal cycle. Fig. 9 presents the spatial distribution of diurnal phase and amplitude of wind speed averaged during the period from November 2018 to March 2019 according to mean maximum hourly wind speed within the 24 h. The occurrence time of maximum hourly wind speed is marked as early morning (0000–0600 Beijing time, BJT), morning (0600–1200 BJT), afternoon (1200–1800 BJT), and evening (1800–2400 BJT), respectively. To highlight the vertical detection capabilities of wind radar, mean maximum wind speed at four different heights above ground level (500, 1000, 1500 and 2500 m) are investigated. As shown in the Fig. 9a (at 500 m), among the 106 observational sites, mean maximum wind speed occurs in the morning at 76 sites (about 71.9%), followed by 12 sites (11.3%) with peaks in the early morning. On the other hand, only 6 sites (5.5%) have an afternoon peak, whereas 12 sites (11.3%) have an evening peak. The story with respect to the diurnal phase and amplitude of mean maximum wind speed at other heights is almost the same (Fig. 9b-d). In terms of vertical direction, the occurrence timing of mean maximum wind speed at most stations is consistent; but some stations of northwest China (Wulumuqi, Lanzhou and Qinghai) show a different pattern. Moreover, the amplitude of mean maximum wind speed at 2500 m height is two or three times than that at other height, indicative that the maximum wind speed increases with the height. In terms of the spatial pattern, mean maximum wind speed generally occurs in the morning in the coastal region of eastern China, with magnitude generally lower than 10 m/s. By comparison, both early morning and afternoon peaks contribute almost equally to the diurnal cycle in the inland region.

4.2 Regional wind field analysis

The wind profile data can also be used to investigate the regional wind field. As shown in Fig. 10, there are a total of 11 regions of interest (ROIs) selected for further analysis on the regional wind characteristics according to the spatial distribution of RWP stations as well as land cover (Table 2). The land cover types data is obtained from the Moderate-resolution Imaging Spectroradiometer (MODIS). The MODIS Land Cover product is derived through a supervised decision-tree classification method. The land cover types are divided into 17 classes, including 11 natural vegetation classes, three human-altered classes, and three non-vegetated classes (Friedl et al., 2019). Fig. 10 shows the atmospheric wind field variation of each ROI at 500 m above ground level during the study period. From the perspective of wind direction, the North China Plain is mainly southwest wind during the study period, the southwest wind at ROI 3 and 4 accounted for 40.3% and 48% respectively. The south China area is mainly dominated by northeast wind, such as ROI 8, 9, 10, and 11. The distribution of wind direction over central China is more uniform. Western China is dominated by northwest wind, and the percentages of northwest wind at ROI 1 is 45.8%. In terms of the spatial pattern wind speed, the wind speed in western China is relatively low. The percentages of wind speed less than 4 m/s at ROI 1, 5, and 7 are 76.2%, 78.7%, and 83.2%, respectively. Moreover, the land cover type of ROI 1, 5, and 7 is grassland. By contrast, the wind speed in the central and eastern regions is significantly large, and 60% of the wind speed in most ROI can reach 6 m/s. Especially in coastal areas, such as ROI 4 and 9, 30% of wind speed is larger than 8 m/s over the whole study period.

In the long run, the accumulation of more wind profile measurements across China, especially in the lowest part of PBL, will provide a valuable benchmark database for assessment of wind power potentials and be useful for numerical weather prediction (Ishihara et al., 2006; Yim et al., 2007). The policymakers will determine whether the wind turbines (60-100 m above ground level) will be installed or not, aided by high-resolution model simulation analyses. Moreover, the real-time wind field data can be used to predict typhoon and sandstorm paths (Ishihara et al., 2006; Huuskonen et al., 2014).

The RWP network of China can provide powerful data support for disaster warning and air pollution prevention.

5 Concluding remarks

The wind profiles are of great importance to the accuracy of numerical weather prediction model, the prediction of precipitation, the diffusion of air pollution, research on regional climate changes, and site selection of wind power plants. To the best of our knowledge, we for the first time reported on the height-resolved winds starting from ground surface to as high as 3-10 km, based on the RWP network of China, which consists of more than 100 RWP stations. It can provide the vertical profiles of horizontal wind direction, horizontal wind speed, and vertical wind speed. Then, the availability of the RWP network is investigated from system performance index and data accuracy. The evaluation criteria are that the effective detection height reachs 3 km, the data acquisition rate exceeds 60%, and the data confidence is 100%. In addition, in terms of data accuracy, the MMSD is better less than 4 m/s and RMSD is less than 6 m/s. Under this criterion, the availability of the RWP network of China is 84%, which 89 stations are recommended, and 17 stations are not recommended. Finally, the wind profile data has a wide range of applications, such as daily maximum winds detection and regional atmospheric wind field research. This RWP network would serve as a key data source on spatiotemporal distribution of atmospheric wind field in support of scientific researches related to renewable energy, severe weather, climate and climate change in the future.

Data availability

The radar wind profiler data used in this paper can be provided for non-commercial research purposes upon request by email (Dr. Jianping Guo: jpguocams@gmail.com). The ECWMF dataset can be downloaded from https://cds.climate.copernicus.eu/ (last accessed 24 February 2020). Instructions for use and data download methods can be found on the official website.

Author contributions

The study was completed with close cooperation between all authors. J. Guo and B. Liu designed the idea for assessing the radar wind profiler data in China; J. Guo and B. Liu conducted the data analyses and co-wrote the manuscript; L., Shi, Y. Zhang, Y. Ma and W. Gong discussed the experimental results, and all coauthors helped reviewing the manuscript and the revisions.

Competing interests.

The authors declare that they have no conflict of interest.

Acknowledgements.

We are very grateful to the China Meteorological Administration for installment and maintenance of the radar wind profiler observational network. This work was financially supported by the National Key Research and Development Program of China under grants (2017YFC0212600 and 2017YFC1501401), the National Natural Science Foundation of China under grants (41771399, 41401498 and 41627804).

References

Angevine, W. M., White, A. B., and Avery, S. K.: Boundary-layer depth and entrainment zone characterization with a boundary-layer profiler. Boundary-Layer Meteorology, 68(4), 375-385, https://doi.org/10.1007/BF00706797, 1994.

Benjamin, S.G., Schwartz, B.E., Szoke, E.J., and Koch, S.E.: The value of wind profiler data in US weather forecasting. Bulletin of the American Meteorological Society, 85(12), 1871-1886. 2004.

Bianco, L., Wilczak, J. M., and White, A. B.: Convective boundary layer depth estimation from wind profilers: Statistical comparison between an automated algorithm and expert estimations. Journal

of Atmospheric and Oceanic Technology, 25(8), 1397-1413, https://doi.org/10.1175/2008jtecha981.1, 2008.

Chouza, F., Reitebuch, O., Jähn, M., Rahm, S., and Weinzierl, B.: Vertical wind retrieved by airborne lidar and analysis of island induced gravity waves in combination with numerical models and in situ particle measurements, Atmos. Chem. Phys., 16, 4675–4692, doi:10.5194/acp-16-4675-2016, 2016.

Chipilski, H. G., Wang, X., and Parsons, D. B.: Impact of Assimilating PECAN Profilers on the Prediction of Bore-Driven Nocturnal Convection: A Multi-Scale Forecast Evaluation for the 6 July 2015 Case Study. Monthly Weather Review, https://doi.org/10.1175/MWR-D-19-0171.1, 2019.

Constantinescu, E.M., Zavala, V.M., Rocklin, M., Lee, S. and Anitescu, M.: Unit commitment with wind power generation: integrating wind forecast uncertainty and stochastic programming (No. ANL/MCS-TM-309). Argonne National Lab.(ANL), Argonne, IL, United States, 2009.

Dolman, B. K., Reid, I. M., and Tingwell, C.: Stratospheric tropospheric wind profiling radars in the Australian network. Earth, Planets and Space, 70(1), 170, 2018.

Du, Y., Zhang, Q., Ying, Y., and Yang, Y.: Characteristics of low-level jets in Shanghai during the 2008-2009 warm seasons as inferred from radar wind profiler data. Journal of the Meteorological Society of Japan. Ser. II, 90(6), 891-903, 2012.

Dong, B. J., Zhang, Y., Xu, A. L., and Fu, Z. J.: Comparative analysis on wind data from radar wind profiler and balloon sounding. Journal of Yunnan University (in Chinese), 1, 18-25, 2011.

Dibbern, J., W. Monna, J. Nash, and G. Peters: COST Action 76-final report. Development of VHF/UHF wind profilers and vertical sounders for use in European observing systems. European Commission, 350 pp, 2001.

Fan, J., Yuan, T., Comstock, J.M., Ghan, S., Khain, A., Leung, L.R., Li, Z., Martins, V.J. and Ovchinnikov, M.: Dominant role by vertical wind shear in regulating aerosol effects on deep convective clouds. Journal of Geophysical Research: Atmospheres, 114(D22), https://doi.org/10.1029/2009JD012352, 2009.

Friedl, M., Gray, J., Sulla-Menashe, D.: MCD12Q2 MODIS/Terra+Aqua Land Cover Dynamics Yearly L3 Global 500m SIN Grid V006 [Data set]. NASA EOSDIS Land Processes DAAC. https://doi.org/10.5067/MODIS/MCD12Q2.006, 2019.

Guo, J., M. Deng, S. S. Lee, F. Wang, Z. Li, P. Zhai, H. Liu, W. Lv, W. Yao, and X. Li: Delaying precipitation and lightning by air pollution over the Pearl River Delta. Part I: Observational analyses. Journal of Geophysical Research: Atmospheres, 121, 6472–6488, doi:10.1002/2015JD023257, 2016.

Guo, J., He, J., Liu, H., Miao, Y, Liu, H., and Zhai, P.: Impact of various emission control schemes on air quality using WRF-Chem during APEC China 2014. Atmospheric Environment, 140: 311–319, doi:10.1016/j.atmosenv.2016.05.046.s, 2016.

Guo, J., T. Su, D. Chen, J. Wang, Z. Li, Y. Lv, X. Guo, H. Liu, M. Cribb, and P. Zhai: Declining summertime local-scale precipitation frequency over China and the United States, 1981–2012: The disparate roles of aerosols. Geophysical Research Letters, 46(22), 13281-13289. doi: 10.1029/2019GL085442, 2019.

Haseler, J.: Early delivery suite. ECMWF Tech. Memo. 454, 26 pp, 2004.

Hoffmann, L., Günther, G., Li, D., Stein, O., Wu, X., Griessbach, S., Heng, Y., Konopka, P., Müller, R., Vogel, B., and Wright, J. S.: From ERA-Interim to ERA5: the considerable impact of ECMWF's next-generation reanalysis on Lagrangian transport simulations. Atmos. Chem. Phys., 19, 3097–3124, https://doi.org/10.5194/acp-19-3097-2019, 2019.

Holleman, I.: Quality control and verification of weather radar wind profiles. J. Atmos. Oceanic Technol., 22, 1541–1550, 2005.

Huuskonen, A., Saltikoff, E., and Holleman, I.: The operational weather radar network in Europe. Bulletin of the American Meteorological Society, 95(6), 897-907, 2014.

Hu, M., and Li, M.: The development and technologic status of wind profiling radar. Scientia Meteorologica Sinica (in Chinese), 30(5), 724-729, 2010.

Ishihara, M., Kato, Y., Abo, T., Kobayashi, K., and Izumikawa, Y.: Characteristics and performance of the operational wind profiler network of the Japan Meteorological Agency. Journal of the Meteorological Society of Japan. Ser. II, 84(6), 1085-1096, 2006.

Kwon, B. H., Kim, K. H., Campistron, B., Kim, P., Kim, M. S., Kim, S. J., ... and Jo, W. G.: Frontal Wind Fields Obtained from a UHF Radar wind profiler Network. In EGU General Assembly Conference Abstracts (Vol. 20, p. 5878), 2018, April.

Kottayil, A., Mohanakumar, K., Samson, T., Rebello, R., Manoj, M. G., Varadarajan, R., ... and Vasudevan, K.: Validation of 205 MHz radar wind profiler located at Cochin, India, using radiosonde wind measurements. Radio Science, 51(3), 106-117, 2016.

Liu, B., Ma, Y., Gong, W., Zhang, M., & Yang, J. Study of continuous air pollution in winter over Wuhan based on ground-based and satellite observations. Atmospheric Pollution Research, 9(1), 156-165, 2018.

Liu, B., Ma, Y., Guo, J., Gong, W., Zhang, Y., Mao, F., Li, J., Guo, X., and Shi, Y.: Boundary layer heights as derived from ground-based Radar wind profiler in Beijing. IEEE Transactions on Geoscience and Remote Sensing. doi: 10.1109/TGRS.2019.2918301, 2019.

Liu, H., J. He, J. Guo, Y. Miao, J. Yin, Y. Wang, H. Xu, H. Liu, Y. Yan, Y. Li, and P. Zhai: The blue skies in Beijing during APEC 2014: A quantitative assessment of emission control efficiency and

meteorological influence. Atmospheric Environment, 167: 235–244, doi: 10.1016/j.atmosenv.2017.08.032, 2017.

Lux, O., Lemmerz, C., Weiler, F., Marksteiner, U., Witschas, B., Rahm, S., Schäfler, A., and Reitebuch, O.: Airborne wind lidar observations over the North Atlantic in 2016 for the pre-launch validation of the satellite mission Aeolus, Atmos. Meas. Tech., 11, 3297–3322, https://doi.org/10.5194/amt-11-3297-2018, 2018.

Lux, O., Lemmerz, C., Weiler, F., Marksteiner, U., Witschas, B., Rahm, S., Geiss, A., and Reitebuch, O.: Intercomparison of wind observations from ESA's satellite mission Aeolus and the ALADIN Airborne Demonstrator, Atmos. Meas. Tech. Discuss., https://doi.org/10.5194/amt-2019-431, in review, 2020.

LeMone, M. A., Tewari, M., Chen, F., and Dudhia, J.: Objectively determined fair-weather CBL depths in the ARW-WRF model and their comparison to CASES-97 observations. Monthly Weather Review, 141(1), 30-54, 2013.

Le Bouar, E., Petitdidier, M., and Lemaitre, Y.: Retrieval of ageostrophic wind from a radiosounding network and a single ST radar. Quarterly Journal of the Royal Meteorological Society, 124(551), 2435-2464, 1998.

Lee, S.-S., Guo, J., and Li, Z.: Delaying precipitation by air pollution over Pearl River Delta. Part 2: model simulations. Journal of Geophysical Research: Atmospheres, 121, 11,739–11,760, doi: 10.1002/2015JD024362, 2016.

LeMone, M.A., W.M. Angevine, C.S. Bretherton, F. Chen, J. Dudhia, E. Fedorovich, K.B. Katsaros, D.H. Lenschow, L. Mahrt, E.G. Patton, J. Sun, M. Tjernström, and J. Weil: 100 Years of Progress in Boundary Layer Meteorology. Meteorological Monographs, 59, 9.1–9.85, https://doi.org/10.1175/AMSMONOGRAPHS-D-18-0013.1, 2018.

Li, Z., Wang, Y., J. Guo, C. Zhao, M.C. Cribb, X. Dong, J. Fan, D. Gong, J. Huang, M. Jiang, Y. Jiang, S.-S. Lee, H. Li, J. Li, J. Liu, Y. Qian, D. Rosenfeld, S. Shan, Y. Sun, H. Wang, J. Xin, X. Yan, X. Yang, X. Yang, F. Zhang, & Y. Zheng: East Asian study of tropospheric aerosols and their impact on regional clouds, precipitation, and climate (EAST-AIRCPC). Journal of Geophysical Research: Atmospheres, 124, 13026-13054. https://doi.org/10.1029/2019JD030758, 2020.

Michelson, S.A., and Bao, J.W.: Sensitivity of low-level winds simulated by the WRF model in California's Central Valley to uncertainties in the large-scale forcing and soil initialization. Journal of Applied Meteorology and Climatology, 47(12), 3131-3149, 2008.

Miao, Y., Guo, J., Liu, S., Wei, W., Zhang, G., Lin, Y., and Zhai, P.: The climatology of low level jet in Beijing and Guangzhou, China. J. Geophys. Res. Atmos., 123, 2816–2830, doi: 10.1002/2017JD027321, 2018.

Marksteiner, U., Lemmerz, C., Lux, O., Rahm, S., Schäfler, A., Witschas, B., and Reitebuch, O.: Calibrations and Wind Observations of an Airborne Direct-Detection Wind LiDAR Supporting ESA's Aeolus Mission. Remote Sensing, 10, 2056, https://doi.org/10.3390/rs10122056, 2018

Molod, A., Salmun, H., and Dempsey, M.: Estimating planetary boundary layer heights from NOAA profiler network wind profiler data. Journal of Atmospheric and Oceanic Technology, 32(9), 1545-1561, 2015.

Nash, J., and Oakley, T. J.: Development of COST 76 wind profiler network in Europe. Physics and Chemistry of the Earth, Part B, 3(26), 193-199, 2001.

Oakley, T., J. Nash, and M. Turp: CWINDE project office networking European profilers 1997-2000. Proc. of the MST9 and COST76 Workshop. 525-528, 2000.

Pfahl, S., O'Gorman, P. A., and Fischer, E. M.: Understanding the regional pattern of projected future changes in extreme precipitation. Nature Climate Change, 7(6), 423-427, 2017.

Reitebuch, O., Lemmerz, C., Nagel, E., Paffrath, U., Durand, Y., Endemann, M., Fabre, F., Chaloupy, M.: The airborne demonstrator for the direct-detection Doppler wind lidar ALADIN on ADM-Aeolus. Part I: Instrument design and comparison to satellite instrument. Journal of Atmospheric and Oceanic Technology, 26(12), 2501-2515, 2009.

Reitebuch, O.: The spaceborne wind lidar mission ADM-Aeolus. In Atmospheric Physics (pp. 815-827). Springer, Berlin, Heidelberg, 2012.

Sun, X. Z.: Atmosphere Remote-Sensing Sounding System-Radar wind profiler. Modern Radar, 1, 1994.

Singh, N., Solanki, R., Ojha, N., Janssen, R. H., Pozzer, A., Dhaka, S. K.: Boundary layer evolution over the central Himalayas from radio wind profiler and model simulations. Atmospheric Chemistry & Physics, 16(16), 2016.

Serafin, R., and J. M. Wilson: Operational weather radar in the United States: Progress and opportunity. Bull. Amer. Meteor. Soc., 81, 501–518, 2000.

Schlatter, T. W., and Zbar, F. S.: Wind profiler assessment report and recommendations for future use. NOAA/Forecast Systems Laboratory, 1994.

van de Kamp, D.W.: Current status and recent improvements to the Wind Profiler Demonstration Network. Preprints, 26th Int. Conf. on Radar Meteorology, Norman, OK, 24-28 May 1993. Amer. Meteorol. Soc., Boston, 552-554, 1993.

Weber, B.L., D.B. Wuertz, R.G. Strauch, D.A. Merritt, K.P. Moran, D.C. Law, D.W. van de Kamp, R.B. Chadwick, M.H. Ackley, M.F. Barth, N.L. Abshire, P.A. Miller, and T.W. Schlatter: Preliminary evaluation of the first NOAA demonstration network profiler. J. Atmos. Oceanic Technol., 7, 909-918, 1990.

Williams, P.D., and Joshi, M.M.: Intensification of winter transatlantic aviation turbulence in response to climate change. Nature Climate Change, 3, 644–648, 2013.

Yang, Y., Yim, S.H., Haywood, J., Osborne, M., Chan, J.C., Zeng, Z., and Cheng, J.C.: Characteristics of heavy particulate matter pollution events over Hong Kong and their relationships with vertical wind profiles using high-time-resolution Doppler lidar measurements. Journal of Geophysical Research: Atmospheres, 124, 9609–9623, 2019.

Yim, S.H., Fung, J.C., Lau, A.K., and Kot, S.C.: Developing a high-resolution wind map for a complex terrain with a coupled MM5/CALMET system. Journal of Geophysical Research: Atmospheres, 112(D5). https://doi.org/10.1029/2006JD007752, 2007.

Wang, C., Chen, Y., Chen, M., and Shen, J.: Data assimilation of a dense wind profiler network and its impact on convective forecasting. Atmospheric Research, 104880. https://doi.org/10.1016/j.atmosres.2020.104880, 2020.

Weissmann, M., Busen, R., Dörnbrack, A., Rahm, S., and Reitebuch, O.: Targeted Observations with an Airborne Wind Lidar, J. Atmos. Oceanic Technol., 22, 1706–1719, doi:10.1175/JTECH1801.1, 2005.

Witschas, B., Rahm, S., Dörnbrack, A., Wagner, J., and Rapp, M.: Airborne Wind Lidar Measurements of Vertical and Horizontal Winds for the Investigation of Orographically Induced Gravity Waves. J. Atmos. Oceanic Technol., 34, 1371–1386, doi:10.1175/JTECH-D-17-0021.1, 2017.

Zhai, X., Marksteiner, U., Weiler, F., Lemmerz, C., Lux, O., Witschas, B., and Reitebuch, O.: Rayleigh wind retrieval for the ALADIN airborne demonstrator of the Aeolus mission using simulated response calibration. Atmos. Meas. Tech., 13, 445–465, https://doi.org/10.5194/amt-13-445-2020, 2020.

Zhang, Y., J. Guo, Y. Yang, Y. Wang, and S.H.L. Yim: Vertical wind shear modulates particulate matter pollutions: A perspective from Radar wind profiler observations in Beijing, China. Remote Sensing, 12(3), 546; https://doi.org/10.3390/rs12030546, 2020.

Zhang, Y., Xu, Y., Dong, W., Cao, L., and Sparrow, M.: A future climate scenario of regional changes in extreme climate events over China using the PRECIS climate model. Geophysical Research Letters, 33(24), https://doi.org/10.1029/2006GL027229, 2006.

Tables:

Table 1. Instrument information of radar wind profiler network of China

Type of RWP	Identifier	Max detection height	Frequency	# of sites	Manufacturer
High Troposphere (CFL-16)	PA	8-10 km	440-450 MHz	3	CASIC
Low Troposphere (CFL-08)	PB	6-8 km	440-450 MHz	2	CASIC
Boundary layer	LC	3-5 km	1290 MHz	101	CASIC/CETC/CHG

CASIC: China Aerospace Science & Industry Corp.

CETC: China Electronics Technology Group Corp.

CHG: China Huayun Meteorological Technology Group Corp.

Table 2. Statistics of the number of sites and land cover types for the 11 regions of interest (ROI) in Fig. 10.

Region of interest	Number of sites	Land cover types
1	1	Grassland
2	7	Cropland and Forest
3	10	Urban
4	2	Cropland
5	2	Grassland
6	1	Cropland
7	1	Grassland
8	27	Urban
9	2	Cropland and Forest
10	10	Urban
11	19	Urban and Forest

Figures:

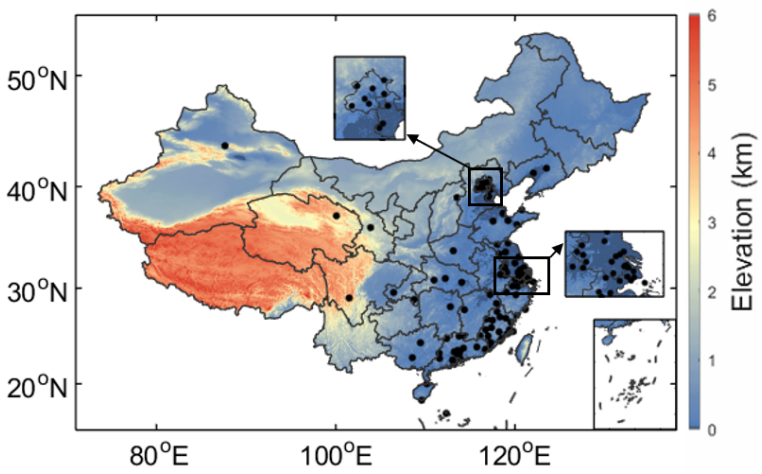

Figure 1. The site distribution of radar wind profiler network of China. Color bar means the elevation.

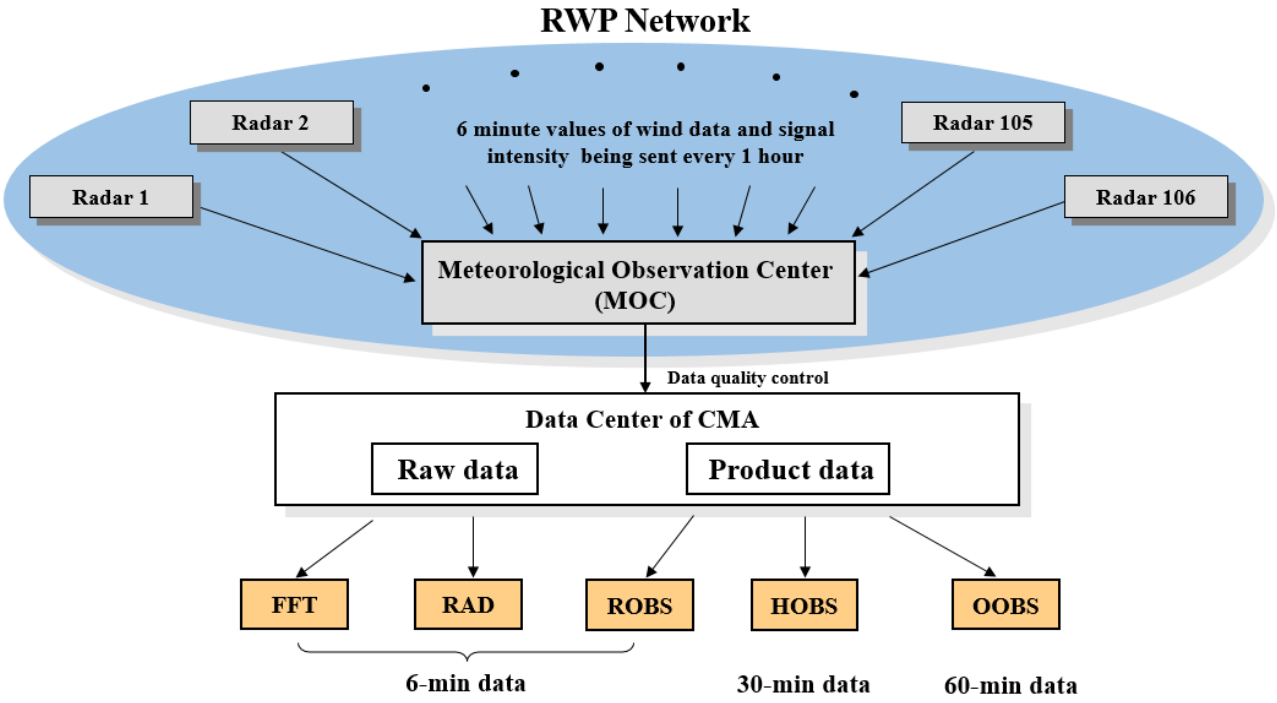

Figure 2. Data transmission framework of radar wind profiler network of China. The RWP network is maintained by the Meteorological Observation Center (MOC), China Meteorological Administration (CMA).

5

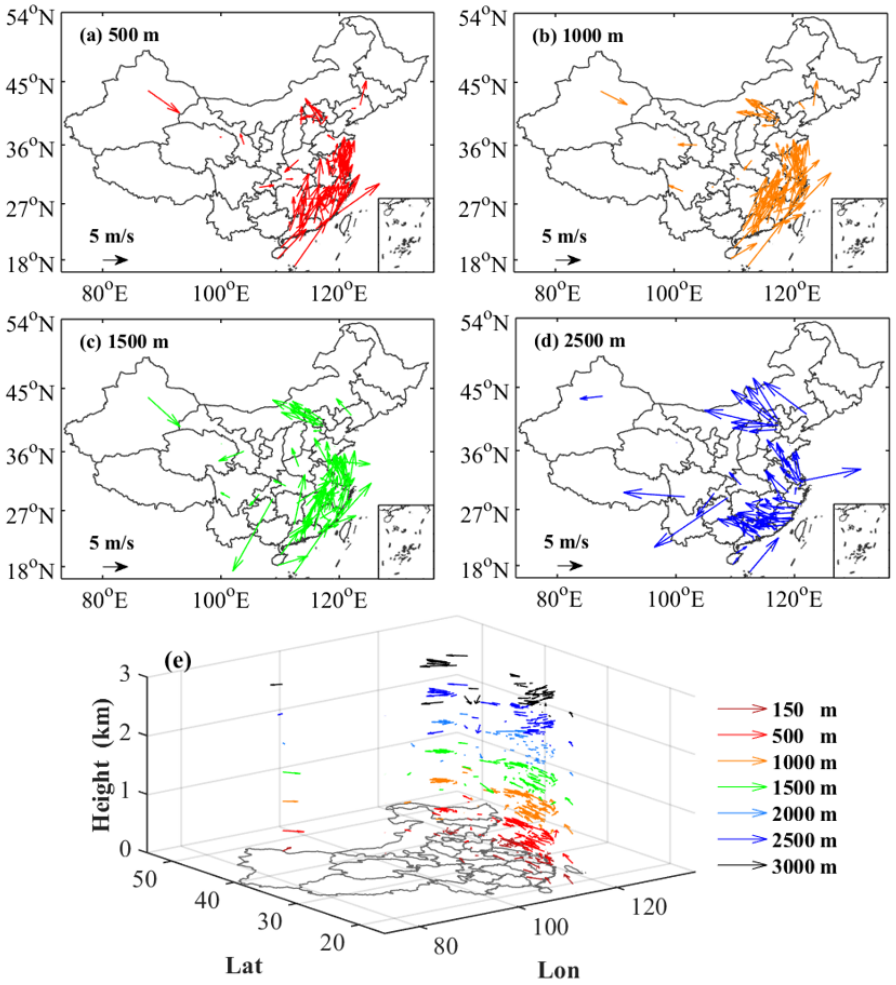

Figure 3. Spatial distribution of average wind field under different height: (a) 500 m, (b) 1000 m, (c) 1500 m, and (d) 2500 m above ground level (AGL). Also shown is (e) the three-dimensional atmospheric wind field observed by the radar wind profiler network of China.

5

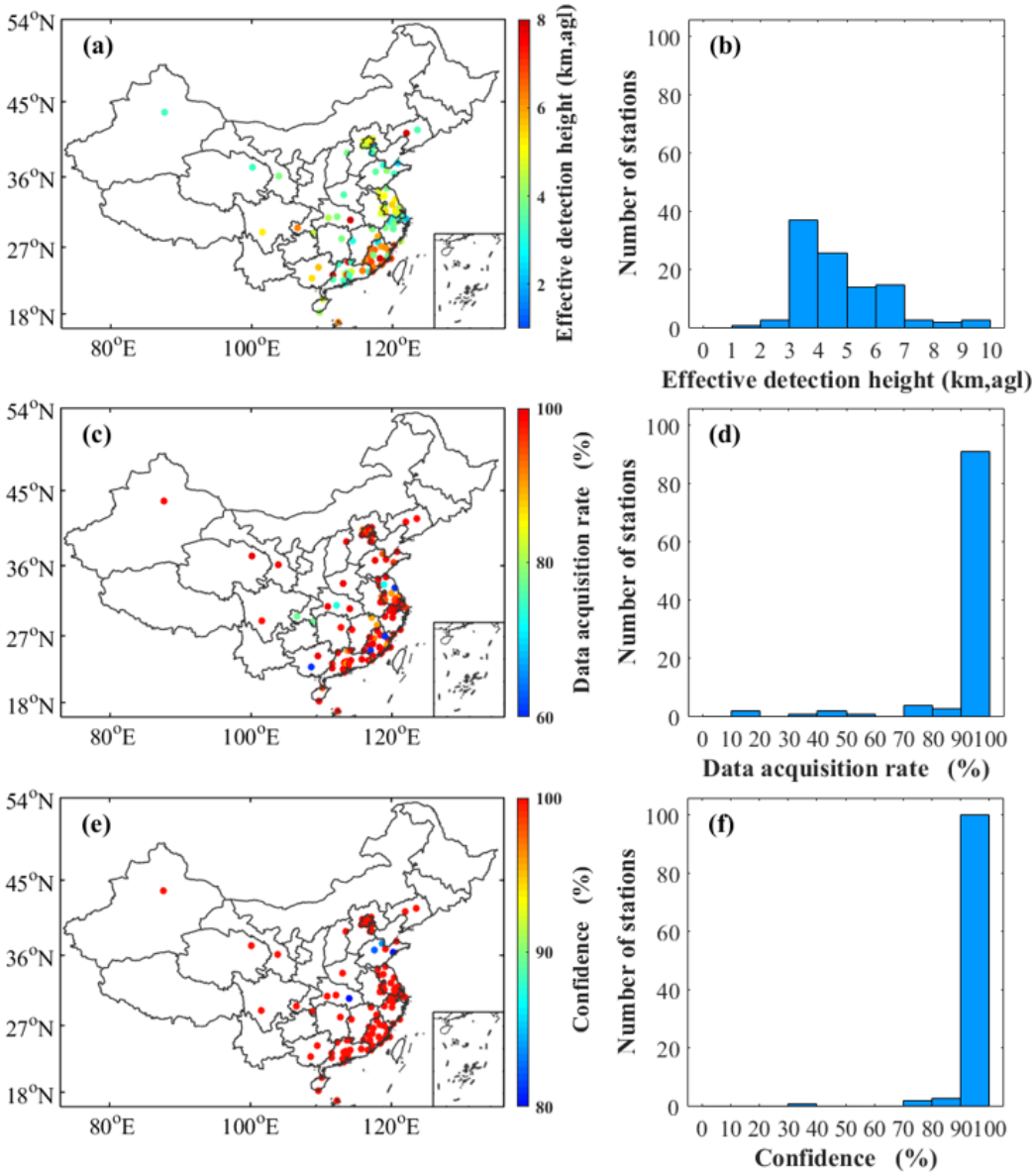

Figure 4. Spatial distribution of (a) mean effective detection height, (c) mean data acquisition rate, and (e) mean data confidence at each station during November 2018 to March 2019; (b), (d), and (f) correspond to the histograms for (a), (c), and (e), respectively.

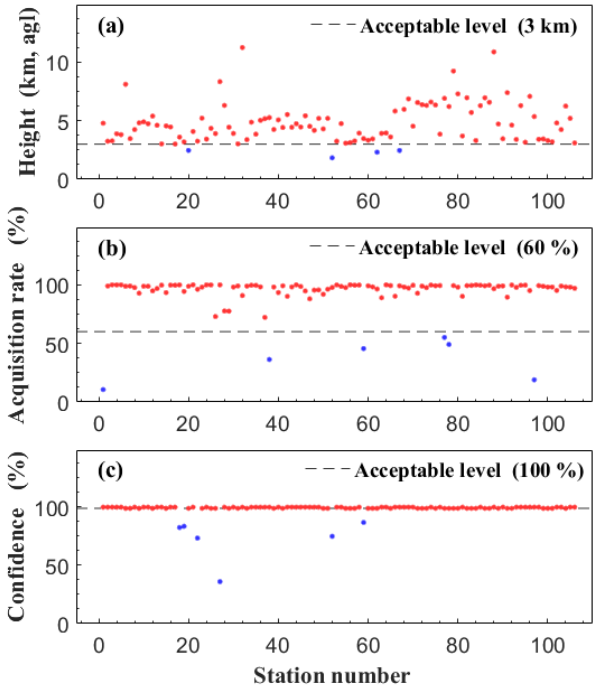

Figure 5. Recommended (red dots) and non-recommended sites (blue dots) of the radar wind profiler network by different performance metrics: (a) effective height detected by RWP, (c) data acquisition rate, and (e) data confidence. The horizontal gray lines indicate their corresponding acceptable threshold levels.

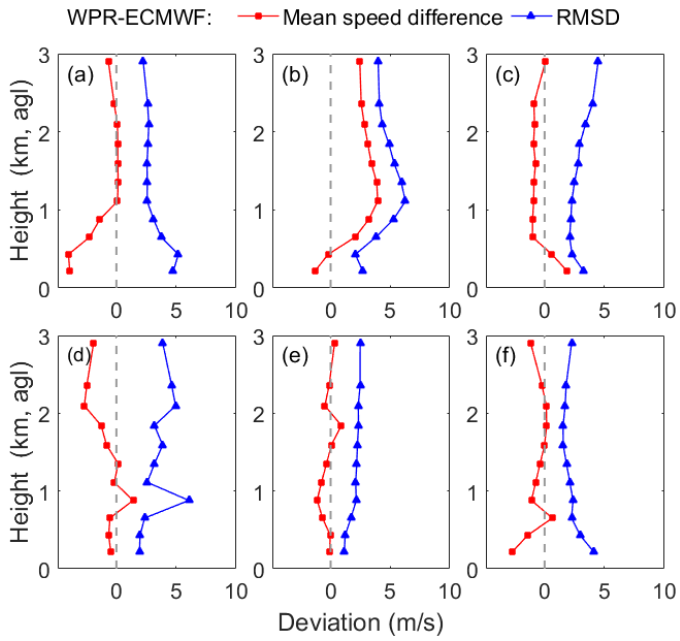

Figure 6. Comparison results between RWP and ECMWF at six RWP stations: (a) Beijing (116°E, 40°N), (b) Wulumuqi (87°E, 43°N), (c) Chongqing (106°E, 30°N), (d) Shanghai (121°E, 31°N), (e) Zigui (111°E, 31°N), and (f) Haikou (110°E, 20°N). The grey, red and blue dot lines represent the the reference line, mean speed difference and root-mean-square difference (RMSD), respectively.

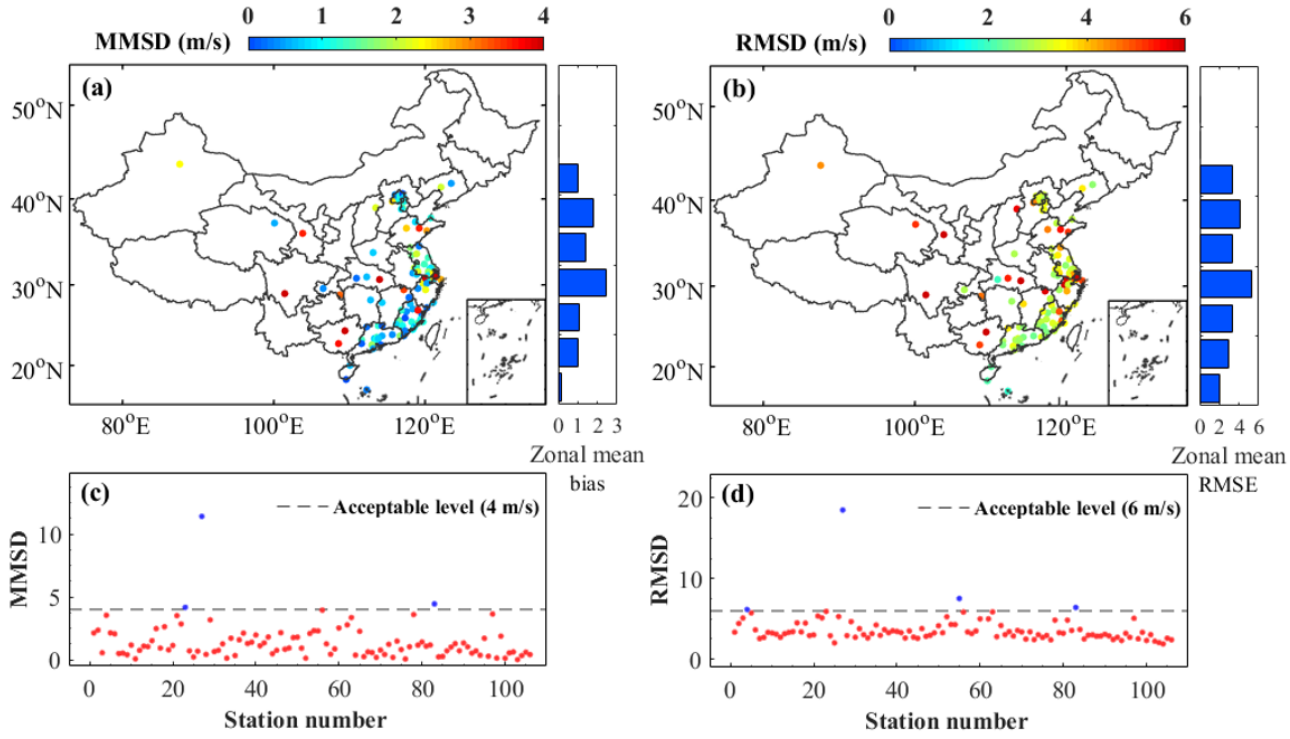

Figure 7. Spatial distribution of (a) magnitude of the mean speed difference (MMSD) and (b) root-mean-square difference (RMSD) at each station during November 2018 to March 2019; the corresponding histogram represent the average difference in zonal direction; (c) and (d) are corresponding recommended (red dots) and non-recommended (blue dots) sites for (a) and (b), respectively. The MMSD and REMD at each station were derived from the measurements over all levels from 0–3 km.

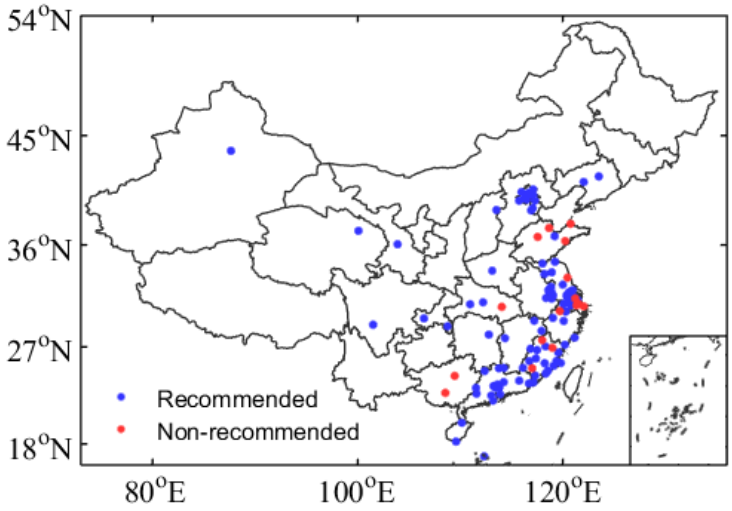

Figure 8. Recommended and non-recommended sites of the radar wind profiler network of China. The blue dots represent the 89 recommended sites and red dots the 17 non-recommended sites.

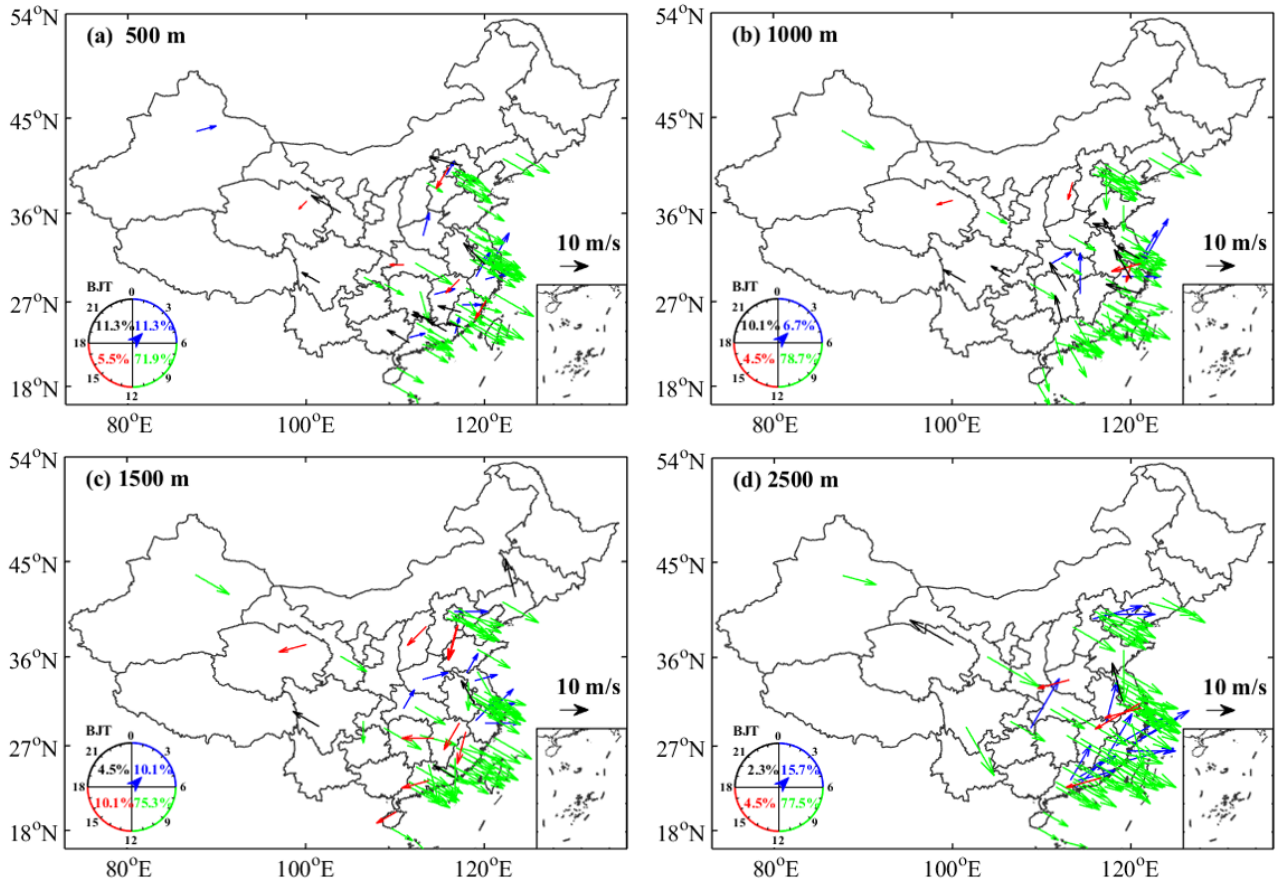

Figure 9. Diurnal phase and amplitude of mean maximum wind speed over the period from November 2018 to March 2019 at (a) 500 m, (b) 1000 m, (c) 1500 m, and (d) 2500 m above ground level (AGL). The direction towards which an arrow points denotes the Beijing time (BJT) when the maximum occurs (shown on the clock dial in the bottom left corner of each panel) and the arrow length represents magnitudes of mean maximum wind speed. The arrow color denotes varying diurnal phases: blue (0000–0600 BJT), green (0600–1200 BJT), red (1200–1800 BJT) and black (1800–2400 BJT).

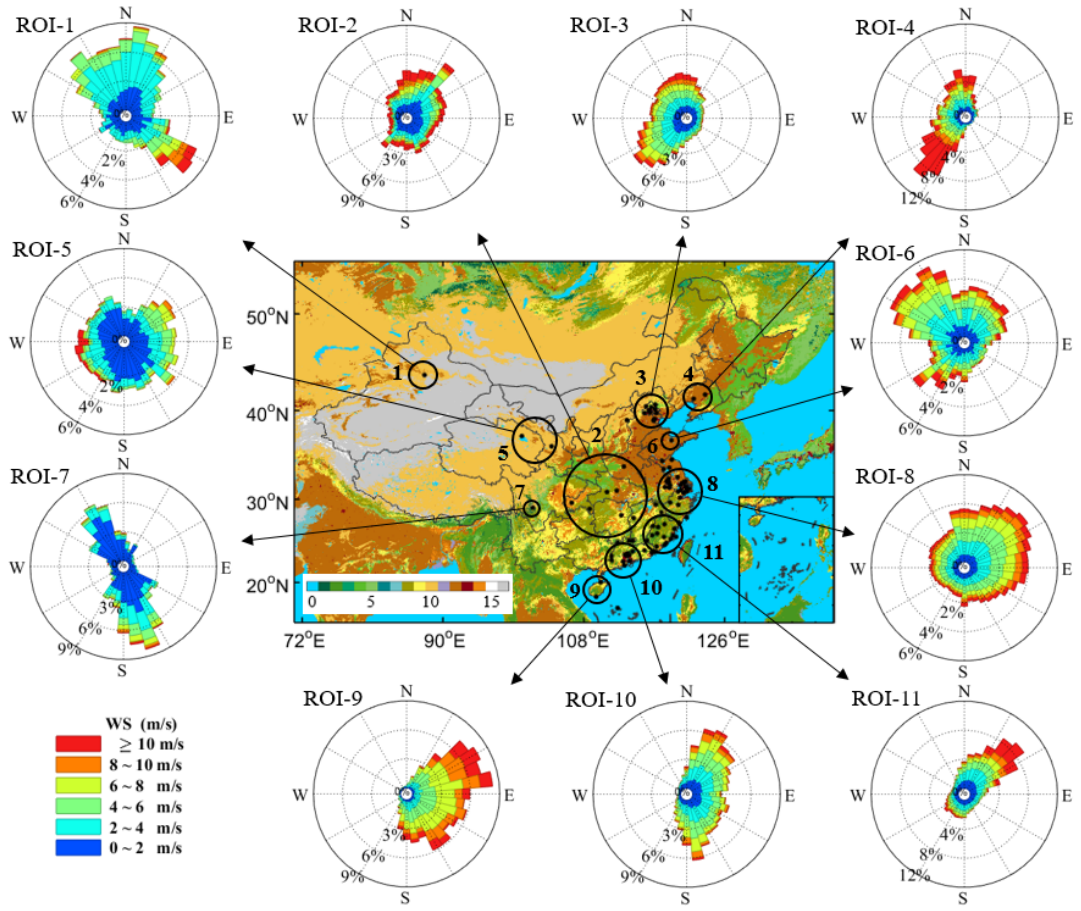

Figure 10. Spatial distribution of the statistical results of atmospheric wind fields at 500 m above ground level (AGL) for 11 regions of interest (ROIs). The wind rose plots over the 11 ROIs are calculated from hourly observations of wind direction and wind speed from November 2018 to March 2019. The land cover types 0–16 represent the Water, Evergreen Needleleaf forest, Evergreen Broadleaf forest, Deciduous Needleleaf forest, Deciduous Broadleaf forest, Mixed forest, Closed shrublands, Open shrublands, woody savannas, Savannas, Grasslands, Permanent Croplands, Urban and built-up, Cropland/Natural vegetation mosaic, Snow and ice, Barren or sparsely vegetated, respectively.